Modeling and Position Control of Tethered Octocopters

Davi Ferreira de Castro*,[a], Igor Afonso Acampora Prado*,[b], and Mateus de Freitas Virgílio Pereira*,[c], Davi Antônio dos Santos*,[d] and José Manoel Balthazar*,[e]
* Aeronautics Institute of Technology, ITA, Brazil.

Abstract. This work presents the modeling and control of a multirotor aerial vehicle with tethered configuration. It is considered an octocopter with a saturated proportional-plus-derivative position control. A viscoelastic model is considered for the tether, which has a tension control. Numerical simulations are carried out to compare the performance of the tethred configuration with the vehicle in free flight.

1 Introduction

Multirotor Aerial Vehicles (MAVs) have been the subject of many academic studies and have attracted a lot of attention from industry in recent years. MAVs have flight capabilities such as hovering, Vertical Take-Off and Landing (VTOL) and agile maneuvering capability, which cannot be achieved by conventional fixed wing aircraft. Some drawbacks of multicopter vehicles are the reduced endurance, which hardly exceeds some minutes and limited payload. Tethered MAVs have been introduced to the aerospace sector as a possible alternative. The tether, even though limiting the vehicle flight range, can be used for data transmission and power supply during operation, which improves the vehicle endurance.

In academia, research works on tethered multicopters are still rare by the present day and there are few companies and institutions that have invested in the development of such vehicles. The first references to consider the tethered configuration are found in [7] and [4]. Some applications of this kind configuration are found in aerostats [1] and robot satellites [2]. The work in [3] presents a navigation strategy in partially mapped environments. This strategy is applied to the collaboration between an UAV [1] and an UGV [2], in which power is provided to the former by a cable connecting the two vehicles. The work [5] presents a strategy to control a tethered helicopter with a combination of classical PID control laws.

This paper presents a modeling and position control strategy for tethered MAV. A viscoelastic model is considered for the cable, in order to reproduce its dynamic behavior. The controller is based on a saturated state feedback control, thus simplifying the controller. This paper is organized as follows: in Section 2 we present the tethered configuration model, in Section 3 a control system is proposed, in Section 4 we present the simulation results and Section 5 presents the conclusions.

[a] e-mail: davifc@ita.br
[b] e-mail: igorap@ita.br
[c] e-mail: mateusfvp@hotmail.com
[d] e-mail: davists@ita.br
[e] e-mail: jmbaltha@ita.br
[1] Unmanned Aerial Vehicle (UAV)
[2] Unmanned Ground Vehicle (UGV)

2 Tethered Configuration Model

This Section presents the multicopter model and tether model, which together describe the dynamics of the tethered multicopter configuration.

2.1 Multicopter Model

Consider a octocopter and three Cartesian coordinate systems (CCS) illustrated in Figure 1.

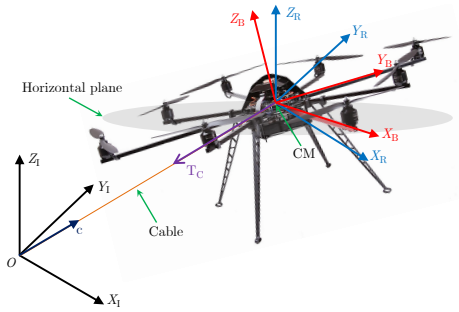

Fig. 1. Cartesian coordinate systems.

The CCS of the body $S_B \triangleq \{X_B,\ Y_B,\ Z_B\}$ is fixed to the vehicle structure and centered on the center of mass (CM). The inertial CCS $S_I \triangleq \{X_I,\ Y_I,\ Z_I\}$ is fixed to the earth at the point O. The CCS $S_R \triangleq \{X_R,\ Y_R,\ Z_R\}$ is parallel to S_I and centered in CM. T_C is tether tension and $\mathbf{c}$ defined tether line vector.

The differential equations that describe the dynamic behavior of the multirotor can be obtained by the Newton-Euler formalism. This work chooses to represent the attitude by the quaternion of rotation $\mathbf{q} \in \mathbb{R}^4$, however for visualization is adopted Euler angles (ϕ, θ and ψ).

The kinematic attitude model for the quaternion of rotation is given by the following differential equation [8]:

$$\dot{\mathbf{q}} = \boldsymbol{\Omega}\mathbf{q} \tag{1}$$

where

$$\boldsymbol{\Omega} = \frac{1}{2}\begin{bmatrix} 0 & -\boldsymbol{\omega}^T \\ \boldsymbol{\omega} & -[\boldsymbol{\omega}\times] \end{bmatrix}, \tag{2}$$

being $\boldsymbol{\omega} \triangleq \left[\omega_x\ \omega_y\ \omega_z\right]^{\mathrm{T}} \in \mathbb{R}^3$ the angular velocity of the vehicle represented in S_{R} and $[\boldsymbol{\omega}\times]$ is given by:

$$[\boldsymbol{\omega}\times] = \begin{bmatrix} 0 & -\omega_z & \omega_y \\ \omega_z & 0 & -\omega_x \\ -\omega_y & \omega_x & 0 \end{bmatrix}. \tag{3}$$

Rewriting the equation (1) explicitly, one obtains:

$$\begin{bmatrix} \dot{q}_1 \\ \dot{q}_2 \\ \dot{q}_3 \\ \dot{q}_4 \end{bmatrix} = \frac{1}{2} \begin{bmatrix} 0 & -\omega_x & -\omega_y & -\omega_z \\ \omega_x & 0 & \omega_z & -\omega_y \\ \omega_y & -\omega_z & 0 & \omega_x \\ \omega_z & \omega_y & -\omega_x & 0 \end{bmatrix} \begin{bmatrix} q_1 \\ q_2 \\ q_3 \\ q_4 \end{bmatrix}. \tag{4}$$

Applying Newton's second law for rotational motion and neglecting disturbance torques, one can obtain:

$$\boldsymbol{\tau} = \dot{\mathbf{h}} + \boldsymbol{\omega} \times \mathbf{h}, \tag{5}$$

where $\boldsymbol{\tau} \triangleq [\tau_x\ \tau_y\ \tau_z]^{\mathrm{T}} \in \mathbb{R}^3$ is the resulting propulsion torque in the vehicle represented in S_{B} and $\mathbf{h} \triangleq \mathbf{I}\,\boldsymbol{\omega} \in \mathbb{R}^3$ is the angular momentum of the body represented in S_{B}, being $\mathbf{I} \in \mathbb{R}^{3x3}$ the matrix of inertia of the vehicle represented in S_{B}. It is assumed that the vehicle has symmetrical structure with respect to the coordinate axes. The matrix $\mathbf{I}$ resulting in a diagonal matrix defined by:

$$\mathbf{I} = \begin{bmatrix} I_x & 0 & 0 \\ 0 & I_y & 0 \\ 0 & 0 & I_z \end{bmatrix}. \tag{6}$$

Rewriting the equation (5) explicitly, one can obtain:

$$\dot{\omega}_x = \frac{(I_y - I_z)}{I_x}\omega_y\omega_z + \frac{\tau_x}{I_x}. \tag{7}$$

$$\dot{\omega}_y = \frac{(I_z - I_x)}{I_y}\omega_x\omega_z + \frac{\tau_y}{I_y}. \tag{8}$$

$$\dot{\omega}_z = \frac{(I_x - I_y)}{I_z}\omega_x\omega_y + \frac{\tau_z}{I_z}. \tag{9}$$

Applying the second Newton's law of motion and neglecting any perturbation, we obtain the following model of translational movement in S_{I}:

$$\ddot{\mathbf{r}} = \frac{1}{m} f\mathbf{n} + \begin{bmatrix} 0 \\ 0 \\ -g \end{bmatrix}, \tag{10}$$

where $\mathbf{r} \triangleq [r_x\ r_y\ r_z]^{\mathrm{T}} \in \mathbb{R}^3$ is the three-dimensional position of the CM represented in S_{I}, $\mathbf{n} \triangleq [n_x\ n_y\ n_z]^{\mathrm{T}} \in \mathbb{R}^3$ is the normal unit vector perpendicular to the rotor plane represented in S_{I}, f is the total thrust, g is the acceleration of gravity and m is the mass of the vehicle.

2.2 Tether Model

A viscoelastic model for the cable is considered in order to reproduce its behavior, as illustrated in Figure 2. More precisely, the model consists of a damper with coefficient d_a and a spring with stiffness k_a in parallel, both connected in series with a spring of different stiffness k_b.

Where x_1 is an unobservable variable which describes the inner friction, x_2 represents the elongation of that segment, L denotes the unstressed tether segment lenght that is reeled out by the ground device and q_9 is deployed tether segment. It is important to note that in the model adopted the mass of the cable is considered negligible in relation to the vehicle mass. The equations and parameters are proposed by Sandino *et al*[5]. The variables that describe the tether state are shown in Figure 2. The transfer function associated tether model is proposed by Sandino *et al*[5] is given by:

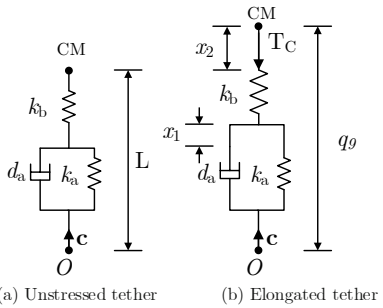

(a) Unstressed tether (b) Elongated tether

Fig. 2. Viscoelastic model of the tether, adapted from [5].

$$\mathrm{G(s)} = \frac{\mathrm{T_C(s)}}{\mathrm{U_C(s)}} = \frac{d_a k_b \left(\frac{k_a}{d_a} + s\right)}{s(k_a + k_b + d_a s)} \tag{11}$$

where $\mathrm{U_C(s)}$ represents the tether velocity of frequency domain. Regarding model parameters d_a, k_a and k_b, they are usually expressed as:

$$k_a = \frac{q.\mathrm{E_1}}{\mathrm{L}},\ k_b = \frac{q.\mathrm{E_2}}{\mathrm{L}},\ d_a = \frac{q.\eta}{\mathrm{L}} \tag{12}$$

Parameter values that have been used in this study for simulation purposes are listed in Table 1.

Table 1. Parameters of the tether model[5].

	Parameter	Value	Units
Diameter	d_C	$10e^{-3}$	m
Cross section	q	$\pi\left(\frac{d_C}{2}\right)^2$	m^2
Modulus of elasticity	E_1	0.194	GPa
	E_1	0.543	GPa
Viscosity	η	0.096	GPa.s
Initial tether length	L	10	m

3 Control System

3.1 Multicopter Control

The multicopter control strategy presented in this section is described by Santos *et al*[6]. Let us define the total thrust vector $\in \mathbb{R}^3$ of the octocopter to be:

$$\mathbf{f} \triangleq f\mathbf{n}. \tag{13}$$

Let us define the inclination angle $\varphi \in \mathbb{R}$ of the octocopter to be:

$$\varphi \triangleq \cos^{-1} n_z. \tag{14}$$

Note that φ consists of the angle between $\mathbf{n}$ and Z_R (see Figure 3).

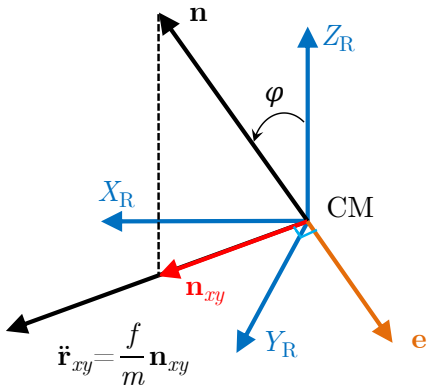

Fig. 3. Relationship between the normal unit vector $\mathbf{n}$ and the horizontal acceleration $\ddot{\mathbf{r}}_{xy}$.

Let $\bar{\mathbf{r}} \triangleq [\bar{r}_x\ \bar{r}_y\ \bar{r}_z]^\mathrm{T} \in \mathbb{R}^3$ denote the position desired for the octocopter and define the corresponding tracking error $\tilde{\mathbf{r}}^{(i)} \in \mathbb{R}^3$ by

$$\tilde{\mathbf{r}} \triangleq \mathbf{r} - \bar{\mathbf{r}}. \tag{15}$$

Let $\varphi_{\max} \in \mathbb{R}$ be the maximum allowable values of the inclination angle φ, $f_{\min} \in \mathbb{R}$ and $f_{\max} \in \mathbb{R}$ be, respectively, the minimum and the maximum allowable values of the total thrust magnitude f. The solution to the problem of position control is to find a feedback control law for $\mathbf{f}$, which make $\mathbf{r} \to \bar{\mathbf{r}}$ or $\tilde{\mathbf{r}} \to \mathbf{0}$, while respecting the constraints $f_{\min} \leq f \leq f_{\max}$ and $\varphi \leq \varphi_{\max}$. The control position is partitioned into control height and horizontal position control.

3.1.1 Height Control

From Equation (10), the dynamic model of the height of the vehicle r_z is given by

$$\ddot{r}_z = \frac{n_z}{m} f - g. \tag{16}$$

Consider the system modeled by Equation (16), and the minimum $f_{\min} > 0$ and maximum $f_{\max} > f_{\min}$ allowable values of the command total thrust magnitude f. Assume that m, g and $n_z \neq 0$ are exactly known. The feedback control law is given by:

$$f = \begin{cases} f_{\min}, & \alpha_z < f_{\min} \\ \alpha_z, & \alpha_z \in [f_{\min}, f_{\max}] \\ f_{\max}, & \alpha_z > f_{\max} \end{cases} \tag{17}$$

with

$$\alpha_z \triangleq \frac{m}{n_z}\left(g - k_1\left(r_z - r_z\right) - k_2 \dot{r}_z\right), \tag{18}$$

respecting the total thrust magnitude constraint $f_{\min} \leq f \leq f_{\max}$ and is such that if $f_{\min} \leq \alpha_z \leq f_{\max}$, then the vehicle height r_z responds to the height desired $\bar{r}_z$, as if it were governed by the following second order linear time-invariant (LTI) system:

$$\ddot{r}_z + k_2 \dot{r}_z + k_1 r_z = k_1 \bar{r}_z, \tag{19}$$

where $k_1 > 0 \in \mathbb{R}$ e $k_2 > 0 \in \mathbb{R}$ are controller coefficients.

3.1.2 Horizontal Position Control

Let $\mathbf{r}_{xy} \triangleq [r_x\ r_y]^\mathrm{T} \in \mathbb{R}^2$ and $\mathbf{n}_{xy} \triangleq [n_x\ n_y]^\mathrm{T} \in \mathbb{R}^2$ denote the horizontal projections of $\mathbf{r}$ and $\mathbf{n}$, respectively. From equation (10), one can write the horizon position dynamic model as

$$\ddot{\mathbf{r}}_{xy} = \frac{f}{m}\mathbf{n}_{xy}. \tag{20}$$

Consider the system modeled by equation (20) and the maximum allowable value $\varphi_{\max} > 0$ of the inclination angle φ. Assume that m and $f \neq 0$ are exactly known. The feedback control law is given by:

$$\mathbf{n}_{xy} = \begin{cases} \boldsymbol{\alpha}_{xy}, & \|\boldsymbol{\alpha}_{xy}\| \leq \sin\varphi_{\max} \\ \sin\varphi_{\max}\frac{\boldsymbol{\alpha}_{xy}}{\|\boldsymbol{\alpha}_{xy}\|}, & \|\boldsymbol{\alpha}_{xy}\| > \sin\varphi_{\max} \end{cases}, \tag{21}$$

with

$$\boldsymbol{\alpha}_{xy} \triangleq -\frac{m}{f}\left[k_z\left(\mathbf{r}_{xy} - \mathbf{r}_{xy}\right) + k_4 \dot{\mathbf{r}}_{xy}\right], \tag{22}$$

respecting the inclination angle constraint $\varphi \leq \varphi_{\max}$ and is such that if $\|\boldsymbol{\alpha}_{xy}\| \leq \sin\varphi_{\max}$, then $\mathbf{r}_{xy}$ responds to the horizontal position desired $\bar{\mathbf{r}}_{xy} \triangleq [\bar{r}_x\ \bar{r}_y]^\mathrm{T}$ as if it were governed by the following pair of second order LTI systems:

$$\ddot{\mathbf{r}}_{xy} + k_4 \dot{\mathbf{r}}_{xy} + k_3 \mathbf{r}_{xy} = k_3 \bar{\mathbf{r}}_{xy}, \tag{23}$$

where $k_3 > 0 \in \mathbb{R}$ e $k_4 > 0 \in \mathbb{R}$ are controller coefficients.

In practice, the attitude desired for the internal attitude control loops need to be computed from the normal unit vectors $\mathbf{n}$. In order to specify a unique attitude, it is necessary to select a heading. For example, one can choose a zero heading just by taking into consideration the attitude represented by the principal Euler angle/axis $(\varphi, \mathbf{e})$, where φ is the angle of inclination own and $\mathbf{e} \in \mathbb{R}^3$ is a unit vector (see Figure 3) is given by:

$$\mathbf{e} = \frac{\mathbf{n} \times \mathbf{n}_{xy}}{\|\mathbf{n} \times \mathbf{n}_{xy}\|} \tag{24}$$

From $(\varphi, \mathbf{e})$ one can thus represent the attitude of S_B with respect to S_R, using , for example, Euler angles parameterization that permits obtains $\bar{\phi}$, $\bar{\theta}$ and $\bar{\psi}$.

3.2 Tether Tension Control

The tether tension is controlled by a proportional control configuration. The Equation 25 and Figure 4 show the architecture of the tether control, which is described by Sandino *et al*[5].

$$\mathrm{U_C}^\star = k_\mathrm{p}(\mathrm{T_C}^\star - \mathrm{T_C}) \tag{25}$$

where $\mathrm{U_C}^\star$ is the desired velocity tether, $\mathrm{T_C}^\star$ is the desired tether tension and k_p is proportional gain.

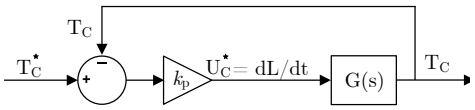

Fig. 4. Control system for simplified tether model given by G(s) is proposed by Sandino *et al*[5].

3.3 Tethered Multicopter Control

In order to control the height, a term T_C was added in Equation 18. Therefore, Equation 26 represents the proposed controller.

$$\alpha_z \triangleq \frac{m}{n_z}\left(g - k_1\left(r_z - r_z\right) - k_2\dot{r}_z\right) + T_C \tag{26}$$

4 Simulation Results

The multicopter dynamics is integrated by using the fourth order Runge-Kutta method with time step of $T = 0.002$ s. The Reference trajectory follows the way-points : $\mathbf{w(1)} = [0\ 0\ 0]^T$m, $\mathbf{w(2)} = [4.24\ 4.24\ 8]^T$m, $\mathbf{w(3)} = [4.24\ -4.24\ 8]^T$m, $\mathbf{w(4)} = [-4.24\ -4.24\ 8]^T$m, $\mathbf{w(5)} = [-4.24\ 4.24\ 8]^T$m and $\mathbf{w(6)} = [4.24\ 4.24\ 8]^T$m. The mass of vehicle is $m = 2.132$ kg and the gravity acceleration is $g = 9.796$ m/s^2. The control parameters of vehicle, k_1, k_2, k_3 and k_4, are chosen based on equations (19) and (23). The maximum overshoot of $M_p^{ref} = 0.02$ m, and a peak time of $t_p^{ref} = 2$ s, were selected, which resulted in $k_1 = 6.29$ and $k_2 = 3.91$. Similarly, the maximum overshoot of $M_p^{ref} = 0.02$ m and a peak time of $t_p^{ref} = 3$ s were selected and the $k_3 = 2.78$ and $k_4 = 2.61$ gains were obtained. The proportional gain tether control selected was $k_p = 0.01$. The simulation was ran for 70 seconds, and the following bounds were selected: $\varphi_{max} = 30°$, $f_{max} = 40$ N e $f_{min} = 2$ N. A sinusoidal disturbance input was added in axes X and Z at $t = 15$s with amplitude of 5N . The simulations provide comparisons between free and tethered flight. The control error was quantified by the root mean square error, given by:

$$E^{RMS} = \sqrt{\frac{1}{3}[(\text{error x})^2 + (\text{error y})^2 + (\text{error z})^2]} \tag{27}$$

Figure 5 presents the position tracking error of the way-points. We can note that the disturbance results in a lower amplitude in the position error for tethered vehicle when compared with the MAV in free flight.

5 Conclusion

This work has presented the modeling and control of a tethered MAV configuration. Numerical simulations showed that, when compared with the traditional vehicle in free flight, the tethered configuration has a better performance under external disturbances. The tether reduces the position error amplitude, improving the robustness of the vehicle. For future work, we consider a lumped mass model for the tether, as well as a pertubation model that corresponds to actual wind profiles in outdoor environments.

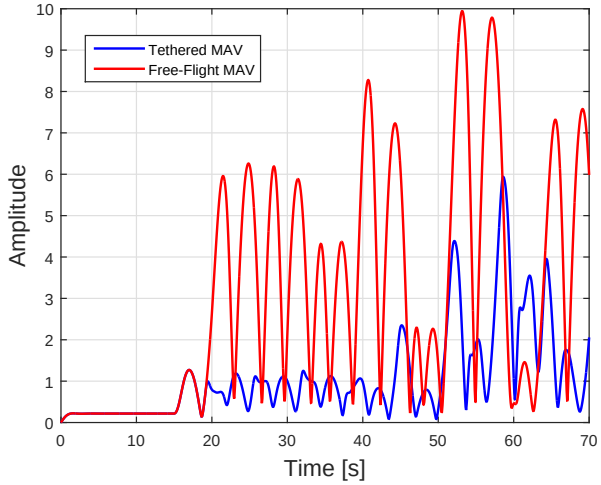

Fig. 5. Position error

Acknowledgements

We would like to thanks Fundação de Amparo à Pesquisa do Amazonas (FAPEAM), Conselho Nacional de Desenvolvimento Científico e Tecnológico (CNPq) and Coordenação de Aperfeiçoamento de Pessoal de Nível Superior (CAPES) for the grants awarded.

References

1. S. Khaleefa, S. Alsamhi, and N. Rajput. Tethered balloon technology for telecommunication, coverage and path loss. IEEE Students Conference on Electrical, Electronics and Computer Science, 2014.
2. M. Nohmi. Mission design of a tethered robot satellite stars for orbital experiment. 18th IEEE International Conference on Control Applications, 2009.
3. C. Papachristos and A. Tzes. The power tethered uav ugv team: A collaborative strategy for navigation in partially mapped environments. 22nd Mediterranean Conference on Control and Automation (MED), 2014.
4. D. Rye. Longitudinal stability of a hovering tethered rotorcraft. *Journal of Guindance, Control and Dynamics*, 8:743–752, 1985.
5. L. A. Sandino, M. Bejar, K. Kondak, and A. Ollero. Advances in Modeling and Control of Tethered Unmanned Helicopters to Enhance Hovering Performance. *Journal of Intelligent and Robotic Systems*, 73:3–18, 2014.
6. D. A. Santos, O. Saotome, and A. Cela. Position Formation Control of Multirotors using Thrust Vector Constraints. *IEEE Transactions on Aerospace and Electronic Systems*, 2013.
7. G. Schmidt and R. Swik. Automatic hover control of an unmanned tethered rotoplatform. *Automatica*, 10:393–403, 1974.
8. J. R. Wertz. *Spacecraft Attitude Determination and control*. Kluwer Academic Publishers, The Netherlands, 1978.